MKKS/BBS6, a divergent chaperonin-like protein linked to the obesity disorder Bardet-Biedl syndrome, is a novel centrosomal component required for cytokinesis

Jun Chul Kim[1], Young Y. Ou[2], Jose L. Badano[3], Muneer A. Esmail[1], Carmen C. Leitch[3], Elsa Fiedrich[1], Philip L. Beales[4], John M. Archibald[5], Nicholas Katsanis[3], Jerome B. Rattner[2] and Michel R. Leroux[1,*]

[1]Department of Molecular Biology and Biochemistry, Simon Fraser University, 8888 University Drive, Burnaby, BC, V5A 1S6, Canada
[2]Department of Cell Biology and Anatomy, University of Calgary, 3330 Hospital Drive NW, Calgary, AB, T2N 4N1, Canada
[3]Institute of Genetic Medicine and Wilmer Eye Institute, Johns Hopkins University, North Wolfe Street, Baltimore, MD 21287, USA
[4]Molecular Medicine Unit, Institute of Child Health, University College London, London, WC1 1EH, UK
[5]Department of Biochemistry and Molecular Biology, Dalhousie University, 5850 College Street, Halifax, NS, B3H 1X5, Canada
*Author for correspondence (e-mail: leroux@sfu.ca)

Accepted 8 December 2004
Journal of Cell Science 118, 1007-1020 Published by The Company of Biologists 2005
doi:10.1242/jcs.01676

Summary

Chaperonins are multisubunit, cylinder-shaped molecular chaperones involved in folding newly synthesized polypeptides. Here we show that MKKS/BBS6, one of several proteins associated with Bardet-Biedl syndrome (BBS), is a Group II chaperonin-like protein that has evolved recently in animals from a subunit of the eukaryotic chaperonin CCT/TRiC, and diverged rapidly to acquire distinct functions. Unlike other chaperonins, cytosolic BBS6 does not oligomerize, and the majority of BBS6 resides within the pericentriolar material (PCM), a proteinaceous tube surrounding centrioles. During interphase, BBS6 is confined to the lateral surfaces of the PCM but during mitosis it relocalizes throughout the PCM and is found at the intercellular bridge. Its predicted substrate-binding apical domain is sufficient for centrosomal association, and several patient-derived mutations in this domain cause mislocalization of BBS6. Consistent with an important centrosomal function, silencing of the *BBS6* transcript by RNA interference in different cell types leads to multinucleate and multicentrosomal cells with cytokinesis defects. The restricted tissue distribution of BBS6 further suggests that it may play important roles in ciliated epithelial tissues, which is consistent with the probable functions of BBS proteins in basal bodies (modified centrioles) and cilia. Our findings provide the first insight into the nature and cellular function of BBS6, and shed light on the potential causes of several ailments, including obesity, retinal degeneration, kidney dysfunction and congenital heart disease.

Key words: Bardet-Biedl syndrome, BBS6, MKKS, Chaperonin, Centrosome, Cytokinesis

Supplementary material available online at
http://jcs.biologists.org/cgi/content/full/118/5/1007/DC1

Introduction

Chaperonins represent a ubiquitous and essential family of sequence and structurally related molecular chaperones required for assisting the folding of newly synthesized, non-native polypeptides (Hartl and Hayer-Hartl, 2002). In bacteria, the chaperonin GroEL is implicated in folding ~10% of all cytoplasmic proteins. Together with endosymbiotically derived mitochondrial Hsp60 and chloroplast cpn60, chaperonins of bacterial origin are classified as Group I (Horwich and Willison, 1993). Their distant relatives, termed Group II chaperonins, are found in the cytosols of eukaryotes and archaea (Gutsche et al., 1999). The eukaryotic cytosolic chaperonin, known as CCT, TRiC or c-cpn, interacts with a range of substrates comparable to that of GroEL, but has also evolved the ability to fold proteins found only in eukaryotes, including actins and tubulins (Leroux and Hartl, 2000; Valpuesta et al., 2002). Both Group I and II chaperonin monomers exhibit a bilobed structure consisting of an ATPase equatorial domain that is joined, via a small intermediate domain, to a substrate-binding apical domain; these in turn typically form double-stacked ring complexes where the apical domains face outwards (Carrascosa et al., 2001).

The three primary distinguishing features of chaperonins are their number of subunits per ring, subunit composition and requirement for a co-chaperone. All Group I chaperonins display sevenfold symmetry and are homo-oligomeric, except for plastid cpn60, which is built from α and β subunits. Their activities depend on a bowl-shaped co-chaperone (GroES) that displaces non-native substrates from the opening of the cavity and encloses them inside a hydrophilic chamber conducive for folding (Hartl and Hayer-Hartl, 2002). Group II chaperonins possess eight different subunits per ring with the exception of some archaeal chaperonins, which have nine (Archibald et al., 1999; Gutsche et al., 1999). The eight subunits of CCT display

~30% amino acid sequence identity to each other, at least as much to archaeal chaperonins, and significantly less (~15%) to Group I chaperonins (Kubota et al., 1995). The different CCT apical domains provide the specificity for CCT to interact with particular substrates through multivalent interactions (Leroux and Hartl, 2000). Another unique property of Group II chaperonins is the presence of a flexible protrusion in the apical domain that serves, in the oligomer, to gate substrate entry and release. This opening and closing of the cavity relies on the ATPase cycle of the chaperonin, which is essential for activity (Meyer et al., 2003). Lastly, prefoldin, a jellyfish-shaped chaperone, cooperates with Group II chaperonins to assist protein folding (Siegers et al., 1999; Siegert et al., 2000; Vainberg et al., 1998).

Until recently, eukaryotes were assumed to harbor one cytosolic chaperonin, CCT. A novel gene mutated in a rare human developmental disease causing hydrometrocolpos, polydactyly and congenital heart disease, McKusick-Kaufman syndrome (MKKS), was identified by Stone et al. (Stone et al., 2000) and found to encode a protein similar to Group II chaperonins. Several mutations in the *MKKS* gene were subsequently associated with Bardet-Biedl syndrome (BBS), a more severe and clinically heterogeneous disease characterized by obesity, retinal degeneration, kidney anomalies, cardiomyopathy, diabetes, polydactyly and other ailments (Katsanis et al., 2000; Slavotinek et al., 2000). Eight genes (*BBS1-8*) are now known to cause BBS, yet only one encodes a chaperonin-like protein, MKKS/BBS6 (Ansley et al., 2003; Badano et al., 2003; Chiang et al., 2004; Fan et al., 2004; Katsanis et al., 2000; Li et al., 2004; Mykytyn et al., 2001; Mykytyn et al., 2002; Nishimura et al., 2001; Slavotinek et al., 2000). Of the BBS proteins, BBS6 is among the least characterized, but there is compelling evidence that all BBS proteins participate in a common cellular process, given that mutations in any *BBS* gene result in clinically indistinguishable phenotypes (Katsanis, 2004).

The most plausible hypothesis regarding a shared function for BBS proteins is that they assist microtubule-related transport and cellular organization processes, in particular relating to ciliary/flagellar and centrosomal activities. This hypothesis is supported by several studies using different model organisms. *Caenorhabditis elegans* BBS-1, 2, 3, 5, 7 and 8 homologues localize at the base of cilia in structures analogous to basal bodies (modified centrioles), and two mutants (*bbs-7* and *bbs-8*) display abnormal ciliary structures and defects in intraflagellar transport, a microtubule- and molecular motor-dependent trafficking activity required for cilia biogenesis and function (Ansley et al., 2003; Blacque et al., 2004; Fan et al., 2004; Li et al., 2004). Similarly, RNA silencing of *Chlamydomonas BBS5* leads to an aflagellar phenotype (Li et al., 2004). Mammalian BBS4, 5 and 8 also localize to centriolar structures, including the centrosome and basal bodies (Ansley et al., 2003; Kim et al., 2004; Li et al., 2004). BBS4 facilitates the transport/targeting of PCM-1 to centrosomes, probably via the $p150^{Glued}$ dynein motor subunit, and its knockdown by RNA interference (RNAi) causes PCM-1 dispersion and microtubule de-anchoring from centrosomes (Kim et al., 2004). A recent study on *BBS4*-null mice suggested that BBS4 is required for sperm flagella production, but the underlying cellular defects remain unclear (Mykytyn et al., 2004). In addition, Kulaga et al. (Kulaga et al., 2004) showed that *BBS1* and *BBS4*-deficient mice possess defects in the structure of olfactory cilia and are anosmic.

Here we provide the first insight into the molecular properties and cellular function of BBS6, and shed light on the molecular etiology of a disease characterized by clinical problems commonly encountered in the general population. We show that BBS6 recently evolved from a CCT subunit and diverged rapidly to acquire specialized functions within the pericentriolar material (PCM) that surrounds centrioles. BBS6 association with the centrosome is independent of the dynein molecular motor, and is conferred by its apical domain. This putative substrate-binding domain is probably important for its in vivo function, as several patient-derived mutations within it cause BBS6 to mislocalize. We also show that BBS6 plays an important role in cytokinesis, and show that it is enriched in tissues that either border, or contain, ciliated cells - consistent with a possible basal body/ciliary function that is shared among all examined BBS proteins.

Materials and Methods

Plasmid constructs

Constructs encoding the full-length, apical domain (amino acids 198-370), or DelGG mutant (Stone et al., 2000) versions of BBS6 were generated by PCR using different sets of 5′ and 3′ primers containing *EcoR*I *and Sal*I restriction sites, respectively, and subcloned into the expression vector pCMV-Myc (Clontech) or pEGFP-C2 (Clontech). pEGFP-C2 empty vector was used to express GFP. The *myc*-tagged p50-dynamitin expression vector was a gift from Richard Vallee. *BBS6* point mutations were generated with the QuickChange Site-Directed Mutagenesis Kit (Stratagene). All constructs were verified by sequencing.

Antibodies

We generated polyclonal antibodies to BBS6 by immunizing rabbits with a 15-mer human BBS6 peptide (GCRIPVDFSSTQILL) conjugated to keyhole limpet hemocyanin (Alberta Peptide Institute, Edmonton). Antibodies were purified using a nitrocellulose membrane-bound human BBS6 protein fragment (amino acids 114-225) encompassing the peptide sequence. The membrane containing the antigen was blocked with 3% BSA in TBS-T (0.05% Tween-20, 100 mM Tris, 150 mM NaCl, pH 7.5) and incubated with crude serum overnight at 4°C. After washing with TBS-T, antibodies were eluted with 0.2 M glycine (pH 2.8) and neutralized with 1 M Tris-HCl, pH 8.0. We also used antibodies to *myc* (ClonTech), GFP (Roche), α-tubulin (Sigma), acetylated tubulin (Sigma), γ-tubulin (Sigma) and CCTα (*StressGen*). The UM1 and PCM1 polyclonal antibodies were kind gifts from Keith Willison (Institute of Cancer Research, London) and Andreas Merdes (University of Edinburgh), respectively. Secondary antibodies to rabbit and mouse IgG were conjugated with Alexa Fluor 488 and 594 (Molecular probes).

Mammalian cell culture

HeLa, NIH 3T3 and COS-7 cells were maintained in DMEM (Gibco, BRL) supplemented with 10% fetal bovine serum (FBS) at 37°C in 5% CO_2. IMCD3 cells were maintained in a 1:1 mixture of DMEM and Ham's F12 medium (Gibco, BRL) with 10% FBS at 37°C in 5% CO_2. For cell synchronization, cells were grown in 2 mM thymidine (Sigma) for 18 hours, washed with PBS and grown in medium without thymidine for 8 hours. Cells were then incubated with 2 mM thymidine for 18 hours, transferred to fresh medium and fixed at various time points to monitor cell cycle progression. For microtubule depolymerization and regrowth, IMCD3 cells were incubated in 25

μM nocodazole at 37°C for 1 hour. Following drug removal, cells were incubated for the indicated time to allow microtubule regrowth. DNA transfections were performed using Polyfect (Qiagen).

Centrosome purification

Centrosomes were isolated using the method described by Ou and Rattner (Ou and Rattner, 2000).

Immunoprecipitations

COS-7 cells were transfected with pEGFP-BBS6 and/or pCMV-Myc-BBS6 and harvested 24 hours after transfection in co-immunoprecipitation (co-IP) buffer (150 mM NaCl, 50 mM TRIS-HCl pH 7.5, 1% NP-40) supplemented with protease inhibitor (Roche). Cell lysates were incubated overnight with 5 μg of anti-CCTα antibody or 10 μg anti-*myc* monoclonal antibody immobilized on sepharose beads (Covance). Immunoprecipitates were washed with co-IP buffer, resuspended in 0.2 M glycine (pH 2.8) and subjected to western blot analysis.

Sucrose gradient fractionation

IMCD3 cells were harvested into 10 ml cold PBS, pelleted and washed in PBS and cold TES buffer (20 mM Tris pH 7.4, 5 mM EDTA, 250 mM Sucrose, 1X protease inhibitor). The final cell pellet was resuspended in 700 μl TES buffer with 1% Triton X-100. Cells in Triton-containing buffer were vortexed and incubated on ice for 30 minutes. 300 μl of cell lysate was loaded on top of discontinuous sucrose gradients comprising 10 steps of 300 μl each, prepared in 20 mM Tris pH 7.4, 10% glycerol, and the appropriate sucrose concentration. Samples were centrifuged at 100,000 ***g*** for 16 hours at 4°C. Fractions (300 μl) collected from the top were subjected to western blot analysis.

Fluorescence microscopy, immunohistochemistry and in situ hybridization

Cells grown on glass coverslips were rinsed in PBS, fixed in –20°C methanol for 10 minutes and blocked in PBS with 5.5% FBS for 60 minutes at room temperature. Cells were then incubated for 60 minutes at room temperature with the relevant primary antibody diluted in PBS. Antibody binding was visualized with Alexa-fluor 488- and 594-conjugated secondary antibodies. Nuclei were counterstained with DAPI. Slides were mounted in Prolong™ anti-fade reagent (Molecular Probes) and observed by fluorescence microscopy using standard epifluorescence, or Leica TCS SP confocal microscope systems. Immunofluorescent digital confocal microscopy and deconvolution were performed as described (Ou and Rattner, 2000). Immunohistochemistry of selected mouse tissues was performed as described previously (Ansley et al., 2003). Whole mount in situ hybridization on murine E10.5-E12 embryos was carried out according to standard protocols using a 1.2 Kb antisense RNA probe specific to the 3′ end of *BBS6*, and its complementary sense probe as a negative control.

Knockdown of *BBS6* expression by RNAi

Knockdown of *BBS6* RNA levels was achieved using the vectors pSilencer™ and pSUPER. pSilencer™ 2.1-U6 neo siRNA expression vector (Ambion) was used to generate an siRNA against *BBS6* by ligating annealed oligonucleotides into *Hin*dIII and *Bam*HI sites; sense: 5′-GATCCCGCAGATTCTGCCTCTGTTGTTCAAGAGACAACAGAGGCAGAATCTGCTTTTTTGGAAA-3′, antisense: 5′-AGCTTTTCCAAAAAAGCAGATTCTGCCTCTGTTGTCTCTTGAACAACAGAGGCAGAATCTGCGG-3′ (underlined is the target sequence corresponding to human *BBS6*). Following transfection, COS-7 cells were subjected to neomycin selection (500 μg activity/ml) for 9 days and then analyzed by microscopy. For construction of the pSUPER vector, sense and antisense oligonucleotides corresponding to mouse *BBS6* were cloned into the pSUPER as described previously (Brummelkamp et al., 2002); sense: 5′-GATCCCCCAGTTATCTCAAGTCTGATTCAAGAGATCAGACTTGAGATAACTGTTTTTGGAAA-3′, antisense: 5′-AGCTTTTCCAAAAACAGTTATCTCAAGTCTGATCTCTTGAATCAGACTTGAGATAACTGGGG-3′ (underlined is the target sequence corresponding to mouse *BBS6*). Transfection, selection and analyses were as with the pSilencer™ vector.

Phylogenetic analyses

BBS6 sequences were added manually to an alignment of Group II chaperonins constructed previously (Archibald et al., 2000). The alignment used for phylogenetic analyses contained 217 unambiguously aligned positions, and corresponded to the regions of the alignment most conserved between BBS6 and Group II chaperonins. Phylogenetic trees were inferred using maximum likelihood (ML) and ML-distance methods. ML trees were constructed with PROML in PHYLIP 3.6 (http://evolution.genetics.washington.edu/phylip.html) using the Dayhoff amino acid substitution matrix, a single randomized sequence-input order, the global rearrangements option and an among-site rate variation model using a six rate category discrete approximation to the Γ distribution plus an additional invariable sites category. TREE-PUZZLE 5.0 (Strimmer and von Haeseler, 1996) was used to estimate relative rates for each category. ML-distance trees were inferred from Γ-corrected distance matrices (calculated using TREE-PUZZLE 5.0, as above) using Fitch-Margoliash (FITCH in PHYLIP 3.6) and BIONJ (Gascuel, 1997). For Fitch-Margoliash analyses, the global rearrangements option was used and the sequence input order was randomized once. Statistical support for ML and ML-distance trees was obtained by bootstrapping. For PROML trees, 100 bootstrap data sets were analyzed using a uniform-rates model, the global rearrangements option and a single randomization of the sequence input order. For the bootstrapping of ML-distance trees, Γ-corrected distance matrices were inferred from 100 re-sampled data sets using PUZZLEBOOT (A. Roger and M. Holder; http://www.tree-puzzle.de), using the parameters described above.

Results

Phylogenetic analysis of BBS6 and Group II chaperonins

To elucidate the evolutionary origin of the single human *BBS6* gene, we constructed phylogenetic trees from an alignment of human and putative mouse, rat, zebrafish and tunicate BBS6 amino acid sequences, as well as Group II chaperonins (CCT subunits and archaeal chaperonins). Results from these analyses, shown in Fig. 1A, indicated that BBS6 sequences are extremely divergent relative to Group II chaperonins. Furthermore, rather than observing an association between BBS6 and archaeal chaperonins, as suggested by the BLAST results of Stone et al. (Stone et al., 2000), our studies suggest a more probable relationship between BBS6 and one of the eukaryotic CCT subunits, CCTα.

The putative BBS6 homologues from *Ciona intestinalis* (sea squirt) and *Danio rerio* cluster with the human, rat and mouse BBS6 proteins with high statistical support. This result is significant as it indicates that BBS6 originated before their divergence and is widespread in animals. The absence of *BBS6* genes from *Caenorhabditis elegans* or *Drosophila melanogaster* further suggests that BBS6 emerged before the

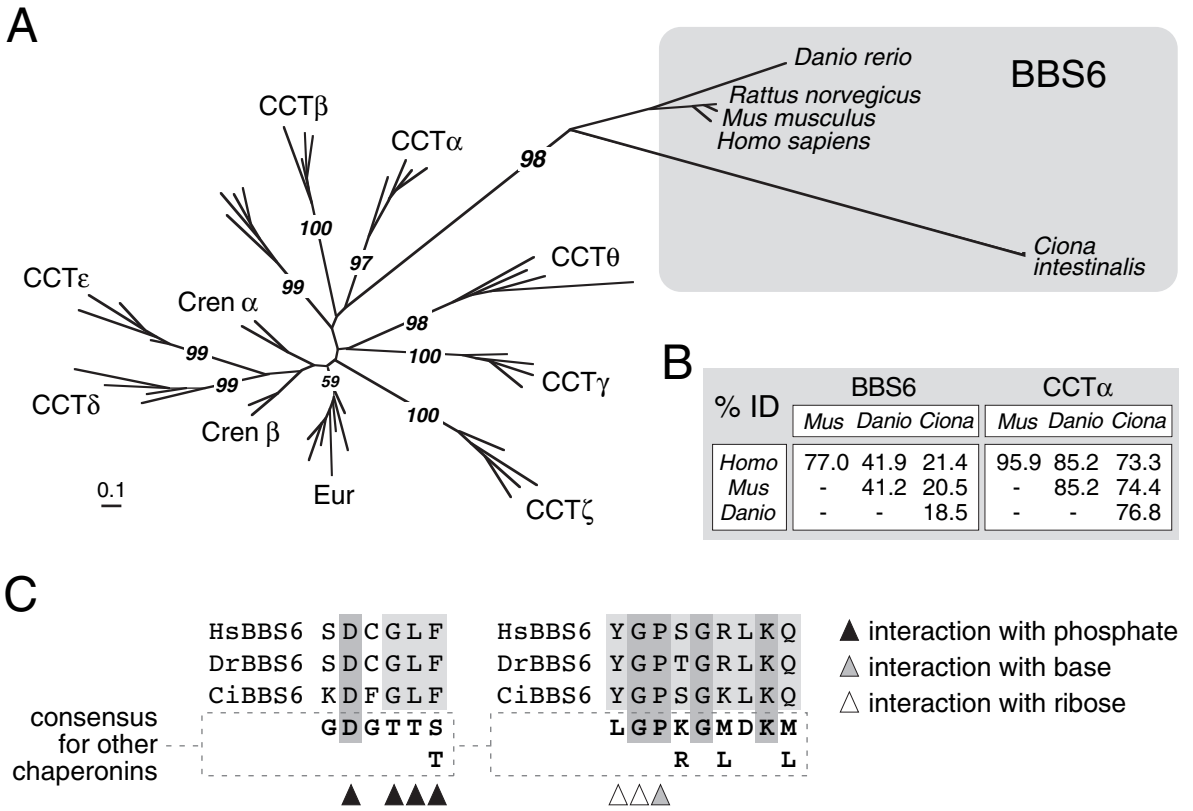

Fig. 1. BBS6 is a highly divergent eukaryotic Group II chaperonin related to CCT. (A) Maximum likelihood phylogenetic tree constructed from an alignment containing 5 BBS6 sequences, 11 archaeal chaperonins and 32 eukaryotic CCTs (four from each of the eight different CCT subunits). The BBS6 sequences are highlighted, and PROML bootstrap support values are provided for significant nodes on the tree where they are >50%. The BBS6 proteins show a weakly supported but consistently observed relationship with the α subunit of CCT, suggesting that the gene encoding BBS6 is a divergent, duplicated CCTα subunit. The scale bar indicates the estimated number of amino acid substitutions per site. Abbreviations: Cren; Crenarchaeotes, Eur; Euryarchaeotes. (B) Amino acid identities shared between *Homo sapiens*, *Mus musculus*, *Danio rerio* and *Ciona intestinalis* BBS6 and CCTα protein sequences. (C) BBS6 proteins share signature sequences that differ from other chaperonins. Alignments of two sequences from human BBS6 (HsBBS6), *Danio* BBS6 (DrBBS6) and *Ciona* BBS6 (CiBBS6) are compared to a consensus sequence derived from CCT and archaeal chaperonins (see Fig. S1 in supplementary material). Positions known to interact with the different regions of the ATP moiety (Ditzel et al., 1998) are indicated with inverted triangles under the alignments.

appearance of vertebrates but after the protostome/deuterostome split. Interestingly, the degree of amino acid sequence identity shared between the BBS6 orthologues suggests that it is evolving much more rapidly than the different CCT orthologues (Fig. 1B). For example, *Homo sapiens* and *C. intestinalis* CCTα share 73.3% amino acid sequence identity, whereas the BBS6 sequences from the same organisms are only 21.4% identical. Likewise, all eight human and mouse CCT orthologues share ~96-97% pairwise identity (Kubota et al., 1995), much greater than the corresponding mammalian BBS6 orthologues (77% identity).

Intriguingly, one of the most conserved Group I and II chaperonin sequences, GDGTT(S/T), which makes several contacts with ATP and is required for its hydrolysis (Ditzel et al., 1998), is significantly different in BBS6 proteins, whereas the corresponding sequences are well conserved between BBS6 from different species (Fig. 1C; see also positions 119-124 in alignment in Fig. S1 in supplementary material alignment). Other residues that are essentially invariant in Group II chaperonins and which are also anticipated to participate in ATP hydrolysis are not conserved in BBS6 proteins (e.g. residues ND in the conserved sequence NDGATIL are SQ, ST or TL in BBS6; positions 88-94 in alignment in Fig. S1 in supplementary material), potentially suggesting differences in ATP binding or hydrolysis. Altogether, these observations indicate that BBS6 has diverged to a much greater degree than have CCT subunits in the same timeframe, and has probably evolved new function(s).

BBS6 is not associated with CCT and is enriched in centrosomal fractions

To provide insight into the cellular distribution and oligomeric nature of BBS6, and to compare its properties to those of other chaperonins, we generated polyclonal antibodies against a short peptide sequence of human BBS6. Following affinity purification, we confirmed the specificity of our antibody by probing a western blot containing extracts from HeLa cells expressing wild-type or *myc*-tagged human BBS6. As shown in Fig. 2A, the anti-BBS6 antibody recognized transiently expressed wild-type (~60 kDa; lane 2) and *myc*-tagged BBS6 (~62 kDa; lane 3). The antibody did not cross-react with

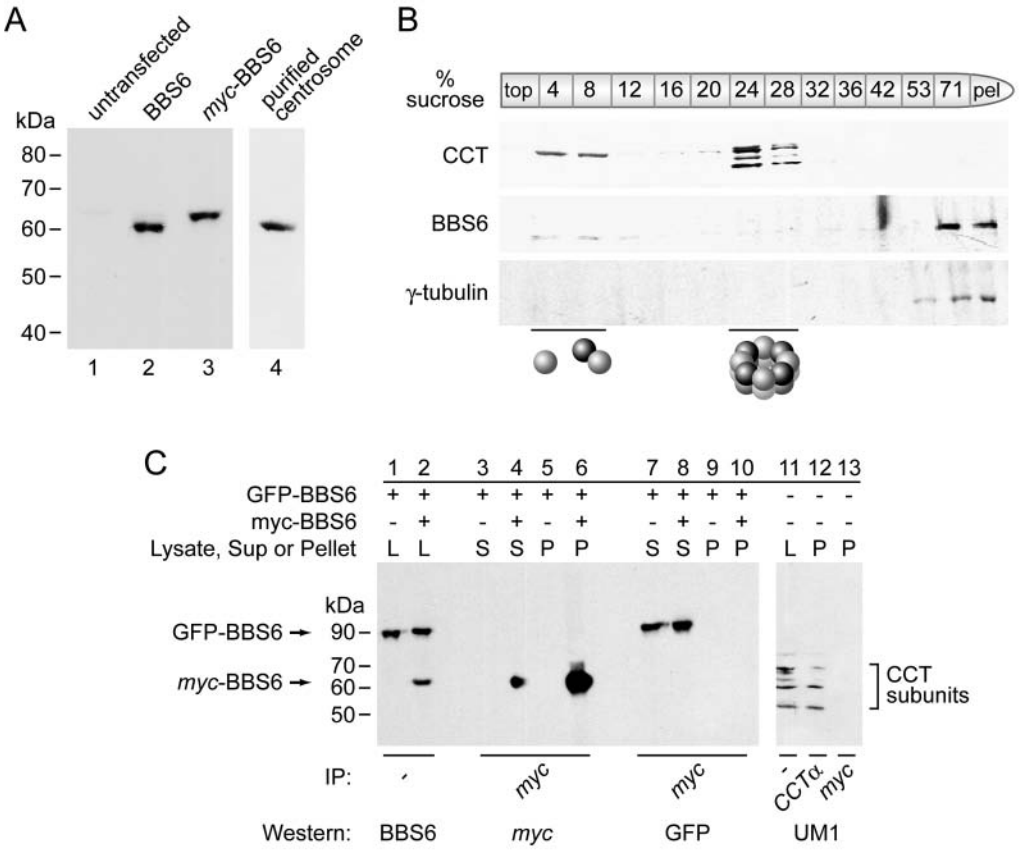

Fig. 2. BBS6 is enriched in centrosomal fractions and its minor soluble form does not associate with CCT or oligomerize. (A) BBS6 is highly enriched in centrosomes purified from NIH 3T3 cells. HeLa cells were either not transfected or transfected with pCMV-Myc-BBS6 or pCMV-BBS6, and total cell lysates were probed by western blot analysis with an affinity-purified polyclonal BBS6 antibody. Wild-type (~60 kDa) and *myc*-tagged BBS6 (~62 kDa) can be observed in the transfected cells. (B) Most of BBS6 occurs as a high-MW Triton X-insoluble form distinct from that of cytosolic CCT. Total lysates of IMCD3 cells expressing pCMV-BBS6 were loaded on discontinuous 4-71% sucrose gradient (the top, bottom and sucrose steps in the gradient are indicated). After centrifugation, each fraction was analyzed on a 10% SDS polyacrylamide gel and subjected to western blot analyses with antibodies to BBS6, CCT or γ-tubulin, as indicated. Most of the BBS6 and γ-tubulin is found in the 71% and pellet fractions, while the majority of CCT forms a peak at ~24% sucrose. Schematics below the panels represent potential positions of monomeric/dimeric or oligomeric chaperonin species. (C) BBS6 does not form homo-oligomers. Extracts of COS-7 cells transiently expressing different constructs (i.e. pEGFP-BBS6 or pCMV-Myc-BBS6, as indicated), or untransfected, were immunoprecitated (IP) with antibodies to *myc*, GFP or CCTα. Lysates (L), immune supernatants (S) or immune pellets (P) were subjected to western blot analyses using antibodies against BBS6, *myc*, GFP or CCT (UM1 antibody), as indicated. The respective positions of *myc*-BBS6, GFP-BBS6 and CCT subunits are noted.

additional proteins, showing its specificity. Endogenous BBS6 was not detected by immunoblot analysis in HeLa cell lysates (Fig. 2A, lane 1), or other mammalian cells (data not shown), due to the low levels of the protein. However, fractionation experiments revealed that a single species of the expected molecular weight (MW) for BBS6 was enriched for, and detected by immunoblotting, in purified centrosomal fractions (Fig. 2A, lane 4).

We next investigated whether BBS6 can form a high-MW oligomer comparable to that of other chaperonins, and whether it might be a transient, minor substituent CCT subunit. Sucrose density gradients were used to compare the sedimentation behavior of transiently expressed wild-type BBS6 to that of endogenous CCT. Lysates from Triton X-disrupted IMCD3 cells were separated on 4-71% discontinuous gradients, and fractions were analyzed by immunoblotting with antibodies recognizing CCT or BBS6. CCT was mainly detected in the 24-28% sucrose fractions, consistent with an expected MW of ~800 kDa (Fig. 2B, top panel). By contrast, the majority of BBS6 sedimented to the 71% sucrose and pellet fractions (Fig. 2B, middle panel). The sedimentation behavior of the transiently expressed BBS6 is probably identical to that of endogenous BBS6, as both of their cellular localization patterns are indistinguishable (see Fig. 3B, below). The bulk of BBS6 co-sedimented with endogenous γ-tubulin, a known centrosomal marker (Fig. 2B, bottom panel). Interestingly, this position on the gradient is comparable to that of BBS4, which was previously shown to associate with the centriolar satellites of centrosomes (Kim et al., 2004).

A small portion of wild-type BBS6 (and *myc*-tagged BBS6; data not shown) sedimented near the top of the gradient (4-8%), as either monomers or small oligomers (Fig. 2B, middle panel). To determine whether BBS6 forms small homo-oligomers (e.g. dimers), we carried out

immunoprecipitation experiments. Equivalent levels of GFP-BBS6 alone, or GFP-BBS6 and *myc*-BBS6 were expressed transiently in COS-7 cells, and supernatants from cell lysates containing the tagged proteins (Fig. 2C, lanes 1 and 2, respectively) were used for immunoprecipitations. These tagged proteins behave identically to that of endogenous BBS6 with respect to their cellular localization pattern, suggesting that the tags do not interfere with their folding (see Fig. 3B, below). An anti-*myc* monoclonal antibody immobilized on sepharose beads efficiently precipitated and enriched for *myc*-BBS6 in cells expressing *myc*-BBS6 but not in cells expressing GFP-BBS6 alone (Fig. 2C, lanes 6 and 5, respectively). However, when GFP-BBS6 was co-expressed with *myc*-BBS6, the anti-*myc* antibody did not precipitate GFP-BBS6, showing that the two tagged BBS6 proteins do not interact (Fig. 2C, lane 10). Importantly, our immunoprecipitation conditions were conducive for precipitating complexes, as an anti-CCTα antibody effectively precipitated the CCT complex, as detected with an antibody (UM1) (Hynes et al., 1995) that recognizes multiple CCT subunits (Fig. 2C, lane 12). Lastly, the lack of interaction between BBS6 monomers was further substantiated by yeast two-hybrid analyses (data not shown).

Together, our biochemical characterization of BBS6 provides evidence that it is not associated with the other known eukaryotic chaperonin, CCT, and that its oligomeric nature – probably that of a monomer – differs from that of chaperonins in general.

BBS6 is found at the centrosome and midbody during cell division

Our fractionation and sedimentation experiments suggested that the bulk of BBS6 is associated with the centrosome, and/or potentially other high-MW, Triton X-insoluble cell component(s). We investigated the cellular localization of BBS6 by fluorescence immunocytochemistry using our affinity-purified anti-BBS6 antibody. Different mammalian cell lines, including human HeLa, murine IMCD3 and NIH 3T3 were fixed and probed with the anti-BBS6 antibody. Endogenous BBS6 was found at two perinuclear focal points in these cells (shown for IMCD3 cells; Fig. 3A). Endogenous BBS6 protein co-localized with γ-tubulin, confirming its centrosomal localization (Fig. 3B, top panels). As further evidence that the BBS6 signal detected by our antibody was specific, we transiently expressed *myc*-BBS6 and GFP-BBS6 in IMCD3 cells and observed that both tagged proteins co-localize with γ-tubulin (Fig. 3B, middle and bottom panels). We also noted that in IMCD3 and NIH 3T3 cells bearing primary cilia, BBS6 is associated with both the daughter and mother centrioles (basal bodies), but is excluded from the ciliary axoneme (Fig. 3C). BBS6 appears to be a core centrosomal protein, as it remains associated with centrosomes during the cell cycle (Fig. 3D). Interestingly, we often observed BBS6 (GFP-tagged and endogenous) at the midbody during cytokinesis (47% of all telophase cells observed, n=178, Fig. 3E), consistent with the fact that several centrosomal proteins are known to localize to the midbody in telophase cells (for example, see Tsvetkov et al., 2003).

Cell-cycle-dependent localization of BBS6 to different regions of the pericentriolar material

To define more precisely the position of BBS6 at the centrosome, we carried out immunolocalization studies of endogenous BBS6 in NIH 3T3 cells using digital confocal microscopy. As shown previously (Fig. 3C), BBS6 was not detected along the axoneme of primary cilia (Fig. 4A). Interestingly, we noted that the immunofluorescence signal of BBS6 may not overlap significantly with γ-tubulin. Instead, one view of BBS6 appeared as distinctive 'O-shaped' structures surrounding γ-tubulin (Fig. 4A), suggesting that BBS6 is part of the PCM tube structure characterized by Ou et al. (Ou et al., 2003). To test this possibility, we co-stained interphase or mitotic cells with our anti-BBS6 antibody and serum (M4491) that specifically recognizes a subset of PCM proteins forming a tube-like structure around centrioles (Mack et al., 1998). BBS6 was consistently found to colocalize with the PCM tube, as seen in side views of representative optical sections (Fig. 4B, lower panels). Interestingly, BBS6 was confined to the lateral walls and excluded from the bottom of the PCM tube in interphase cells (Fig. 4B, upper panels). At the onset of mitosis, BBS6 levels increased and its signal was detected throughout the PCM tube (Fig. 4B, lower panels). BBS6 is therefore a novel centrosomal protein that displays a variable, cell-cycle-dependent localization at the PCM tube.

Centrosomal assembly of BBS6 is independent of microtubules or the dynein motor

We next queried how BBS6 assembles at centrosomes, which serve as nucleation and organizing sites for cytoplasmic microtubules. We first tested whether the association depends on polymerized microtubules. IMCD3 cells were treated with the drug nocodazole, which leads to microtubule depolymerization (Fig. 5A; note the loss of microtubule structures at 0 minutes compared with the no drug control). In nocodazole-treated cells, BBS6 remained centrosomal, as did the core centrosomal protein, γ-tubulin (Fig. 5A; see arrowheads at 0 minutes). This suggested that the association of BBS6 with the centrosome does not depend on polymerized microtubules.

Many centrosomal proteins, including PCM1 and BBS4, are targeted to centrosomes via the microtubule-based dynein-dynactin molecular motor, whereas others (e.g. γ-tubulin) are not (Dammermann et al., 2002; Kim et al., 2004). We therefore investigated whether centrosomal assembly of BBS6 depends on dynein-dynactin by overexpressing p50-dynamitin, which antagonizes the function of the motor in vivo (Vaughan and Vallee, 1995). We confirmed that overexpressing *myc*-tagged p50-dynamitin in IMCD3 cells causes PCM1 mislocalization (in 78% of the transfected cells, n=120, Fig. 5B, left panel). By contrast, just as with γ-tubulin, the centrosomal localization of BBS6 was not affected in cells overexpressing p50-dynamitin (γ-tubulin: 6%, n=150, BBS6: 3%, n=100, Fig. 5B, see arrows in the right and middle panels). From the above results, we conclude that BBS6 is assembled at the centrosome in a microtubule- and dynein-independent manner, as are other integral centrosomal components.

Several BBS6 protein variants found in patients are mislocalized

As protein function depends on correct cell localization, we investigated whether BBS6 missense mutants found in patients fail to localize to centrosomes. Six GFP-tagged BBS6 constructs encompassing mutations in the equatorial, intermediate and apical domains (Fig. 6A) were expressed at similar levels in COS-7 cells (Fig. 6B). As reported above, GFP-tagged wild-type BBS6 is centrosomal in COS-7 cells, and two of the mutant fusion proteins, R156L and C499S also localized properly (Fig. 6C, top panels). However, four mutant proteins, G52D, D285A, T325P and G345E consistently failed to associate with centrosomes (Fig. 6C, bottom panels).

The isolated apical domain of BBS6 is sufficient for centrosomal localization

The mislocalization of three BBS6 variants with missense

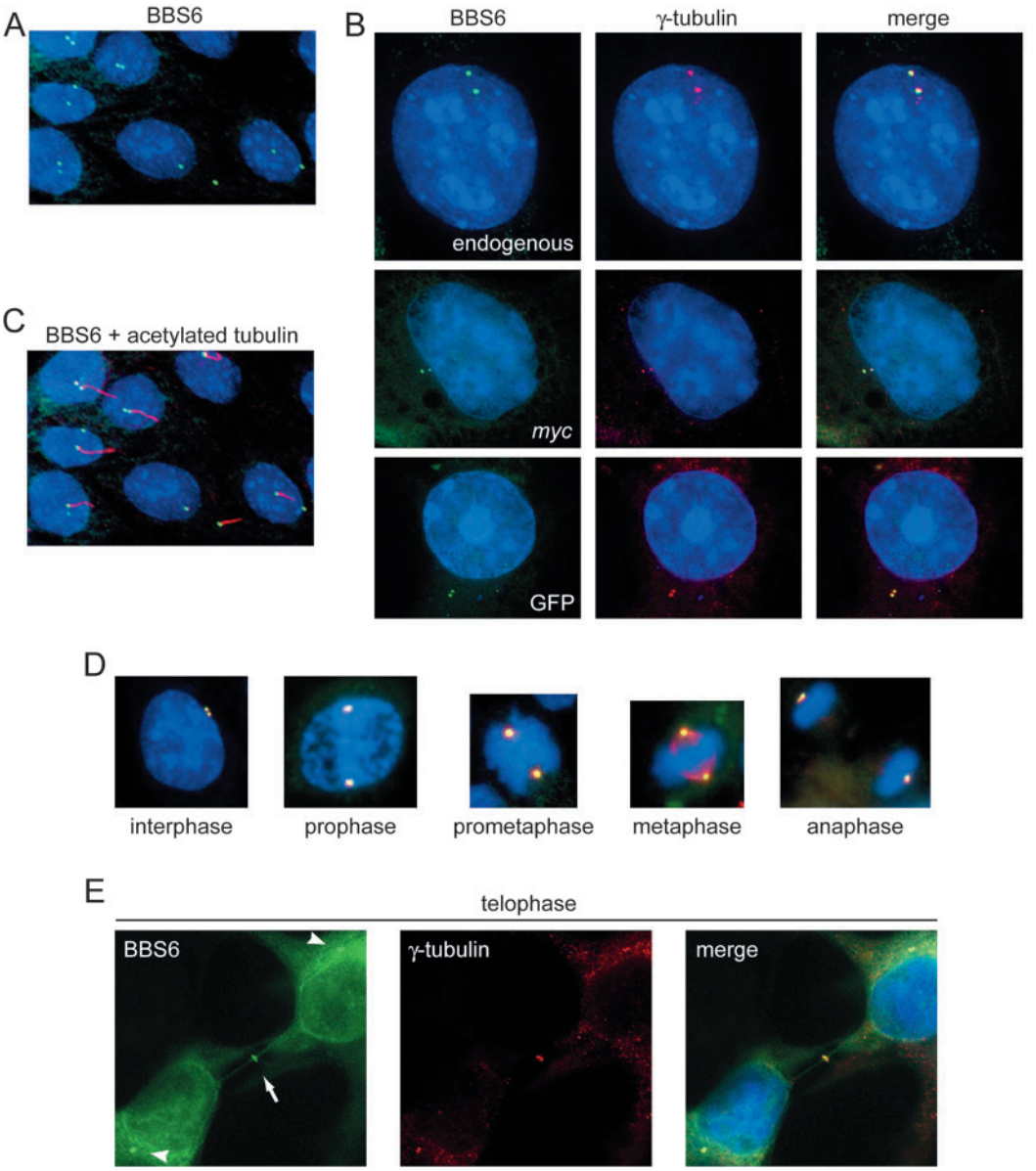

Fig. 3. BBS6 is a centrosomal protein that is also found at the midbody during cytokinesis. (A) Two discrete perinuclear signals are observed in IMCD3 cells by immunocytochemistry using an affinity-purified anti-BBS6 polyclonal antibody. (B) Immunolocalization studies of endogenous BBS6 (top panels) and transiently expressed *myc*-tagged, and GFP-tagged BBS6 (middle and bottom panels, respectively) show that BBS6 colocalizes with the centrosomal marker, γ-tubulin. The transfected cells were fixed and costained with antibodies to *myc* and γ-tubulin, and GFP-BBS6 signal was detected by direct GFP fluorescence (middle and bottom panels). Left, middle and right panels, respectively, show BBS6 (green), γ-tubulin (red) and a merge of the two signals (yellow indicates overlap). (C) Endogenous BBS6 is found at both basal bodies (mother centrioles, displaying a primary cilium) and daughter centrioles. BBS6 is stained green and cilia are stained red with anti-acetylated-tubulin antibodies. (D) BBS6 remains associated with centrosomes throughout the cell cycle. Synchronized IMCD3 cells were co-stained with antibodies to BBS6 (green) and γ-tubulin (red); yellow indicates overlapping signals. (E) BBS6 is found at the centrosomes (indicated by arrowheads) and midbody region (indicated by an arrow) during telophase, as judged by its colocalization with γ-tubulin.

mutations in the apical domain (D285A, T325P and G345E) suggested that this putative substrate-binding domain may be needed to target BBS6 to the centrosome. We tested this possibility by expressing in COS-7 cells a GFP-fusion protein with the apical domain alone (amino acids 198-370; Fig. 6A,B). Similar apical domain fragments have been shown to be stable in isolation and have been crystallized (e.g. the apical domain of CCTγ) (Pappenberger et al., 2002). Remarkably, the

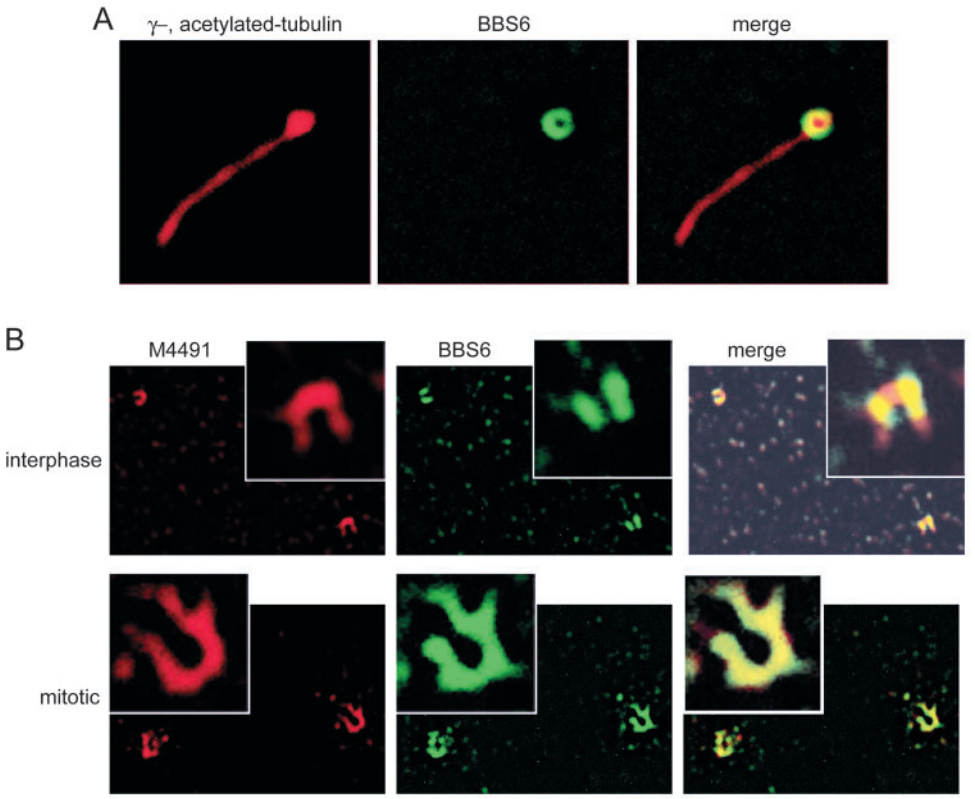

Fig. 4. BBS6 is localized within the pericentriolar material (PCM) tube and shows a dynamic distribution during the cell cycle. (A) High-resolution digital microscopy optical sections of NIH 3T3 cells co-stained with antibodies against BBS6 (green) and γ- and acetylated-tubulin (red). (B) Optical sections of BBS6 (green) and PCM tube (red) signals in the same focal plane from interphase or mitotic HeLa cells. The PCM tube was detected using an antibody, M4491, that recognizes multiple PCM components. Closeups of the PCM tube (insets), BBS6 and merged signals are also shown.

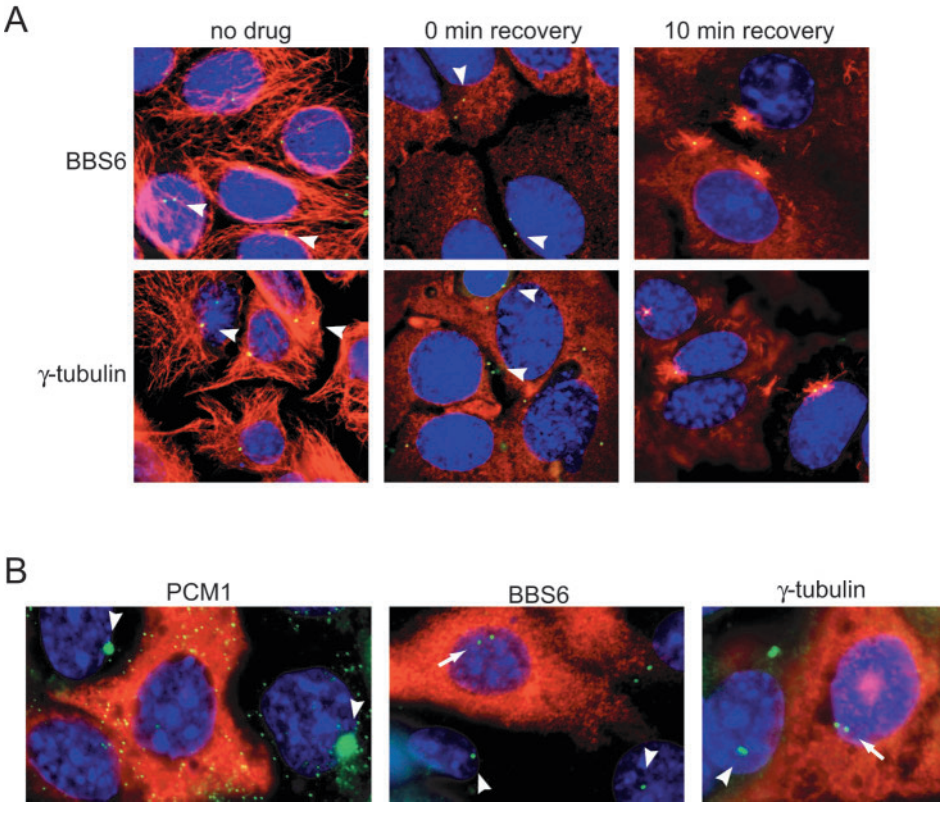

Fig. 5. Centrosomal assembly of BBS6 is not dependent on polymerized microtubules or the dynein-dynactin molecular motor. (A) IMCD3 cells were either mock-treated (no drug) or treated with nocodazole for 1 hour and allowed to recover for 0 or 10 minutes. Cells were then co-stained with antibodies to BBS6 or γ-tubulin (green) and α-tubulin (red). (B) IMCD3 cells were transiently transfected with *myc*-tagged p50-dynamitin, which inhibits dynein-dynactin motor function. Cells were then stained with an anti-*myc* antibody (red) and costained with antibodies to BBS6, PCM1 or γ-tubulin (green). Arrows denote centrosomal BBS6 and γ-tubulin signals from p50-dynamitin-transfected cells, and arrowheads denote centrosomal BBS6, PCM1 and γ-tubulin in untransfected cells. Note the dispersed PCM1 signal in transfected cells.

GFP-tagged BBS6 apical domain associated with the centrosome (Fig. 6D). In addition, we observed that a patient-derived truncated form of the protein that lacks most of the BBS6 C-terminal equatorial domain but retains an intact apical domain (delGG) (see Stone et al., 2000) (Fig. 6A) also localizes normally (Fig. 6D). Taken together, our localization studies on the isolated apical domain and missense/truncation variants show that the BBS6 apical domain region is important for centrosomal localization.

BBS6 silencing by siRNAs causes cytokinesis and other defects

To investigate the cellular function of BBS6, we sought to reduce *BBS6* expression levels in mammalian cells by using RNAi. We transfected COS-7 cells with an expression vector, pSilencer-BBS6, that contains a neomycin resistance gene and a U6 RNA polymerase III promoter, and produces a short interfering RNA (siRNA) specific to the human *BBS6* sequence. Untransfected cells were selected against by incubation in G418-containing media. Real-time quantitative RT-PCR showed that *BBS6* expression was reduced 16-fold compared with control cells containing vector alone (pSilencer-empty).

Phase-contrast microscopic observation of cells transfected with pSilencer-empty vector and pSilencer-BBS6 revealed a conspicuous phenotype for the *BBS6*-silenced cells – namely, that of a large proportion of cells attached by thin intercellular bridges (Fig. 7A, top panels). This suggested that cells had undergone multiple rounds of divisions without completing cytokinesis. Consistent with this observation, a greater percentage of *BBS6*-silenced cells were bi- or multi-nucleated relative to empty vector-transfected control cells (*BBS6* knockdown, 11.9%, *n*=277 cells; control, 5.3%, *n*=300 cells). These results are in agreement with the known role of centrosomes in the resolution of the intercellular bridge (Piel et al., 2001) and the presence of BBS6 in the bridge (Fig. 3E). We also investigated whether the *BBS6*-silenced cells displayed centrosomal anomalies. Staining with the anti-γ-tubulin antibody revealed an increase in the percentage of *BBS6*-silenced cells containing abnormal numbers of centrosomes compared with control cells (greater than four centrosomes in interphase or dividing cells; *BBS6* knockdown, 19.1%, *n*=440; control, 6%, *n*=350; Fig. 7A, top panels). To ensure that these γ-tubulin foci were constituents of bona fide centrosomes, we confirmed by immunofluorescence microscopy that another centrosomal protein (pericentrin) colocalized with the γ-tubulin signals (Fig. S2 in supplementary material). Some *BBS6* knockdown cells lacked centrosomes altogether (data not shown). Importantly, similar results were obtained with two additional siRNA constructs targeted to different regions of the *BBS6* transcript and expressed in the COS-7 cells (data not shown).

To corroborate the results obtained with the COS-7 cells, we conducted similar experiments using a different cell line (NIH 3T3) and a different siRNA expression vector (pSUPER)

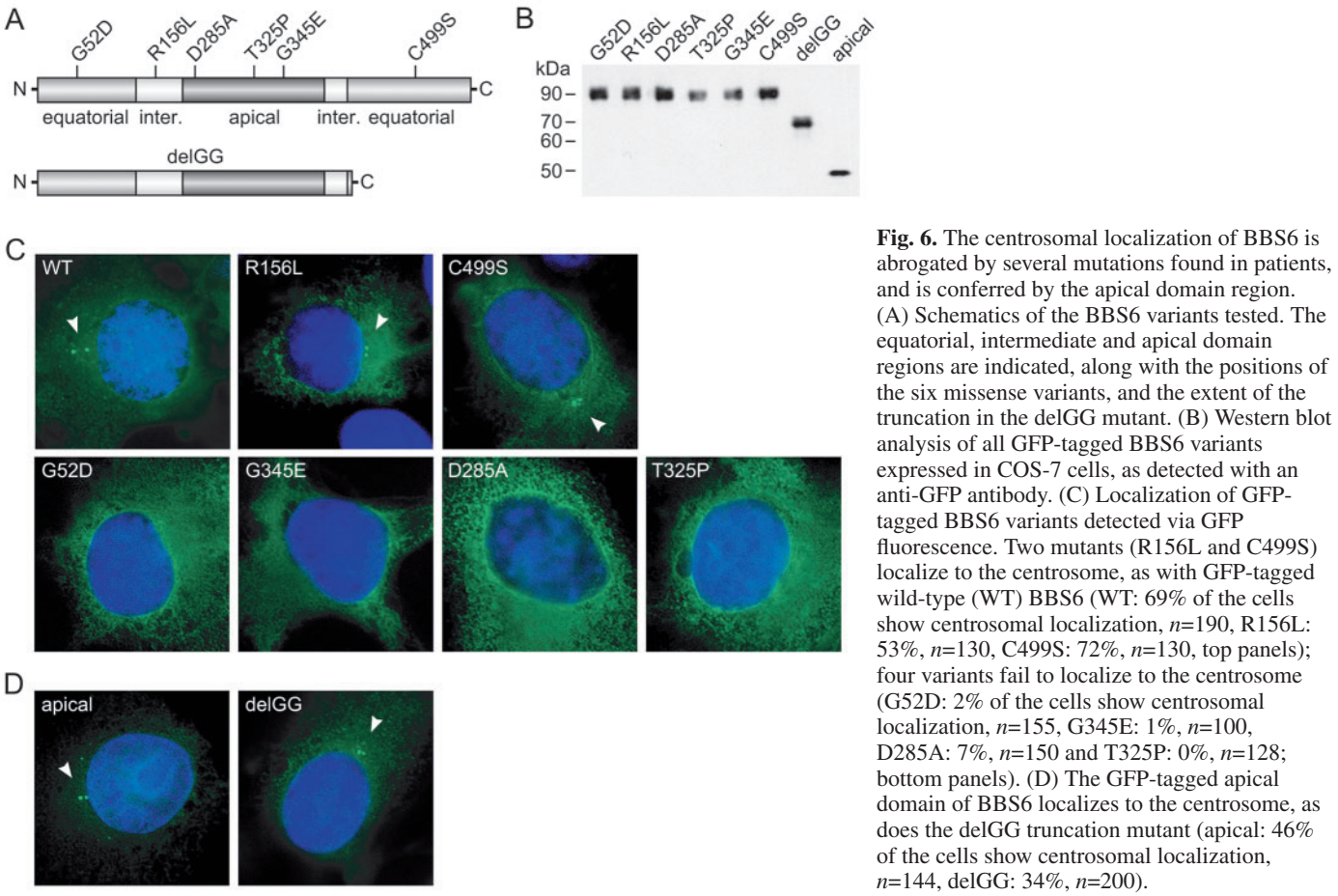

Fig. 6. The centrosomal localization of BBS6 is abrogated by several mutations found in patients, and is conferred by the apical domain region. (A) Schematics of the BBS6 variants tested. The equatorial, intermediate and apical domain regions are indicated, along with the positions of the six missense variants, and the extent of the truncation in the delGG mutant. (B) Western blot analysis of all GFP-tagged BBS6 variants expressed in COS-7 cells, as detected with an anti-GFP antibody. (C) Localization of GFP-tagged BBS6 variants detected via GFP fluorescence. Two mutants (R156L and C499S) localize to the centrosome, as with GFP-tagged wild-type (WT) BBS6 (WT: 69% of the cells show centrosomal localization, *n*=190, R156L: 53%, *n*=130, C499S: 72%, *n*=130, top panels); four variants fail to localize to the centrosome (G52D: 2% of the cells show centrosomal localization, *n*=155, G345E: 1%, *n*=100, D285A: 7%, *n*=150 and T325P: 0%, *n*=128; bottom panels). (D) The GFP-tagged apical domain of BBS6 localizes to the centrosome, as does the delGG truncation mutant (apical: 46% of the cells show centrosomal localization, *n*=144, delGG: 34%, *n*=200).

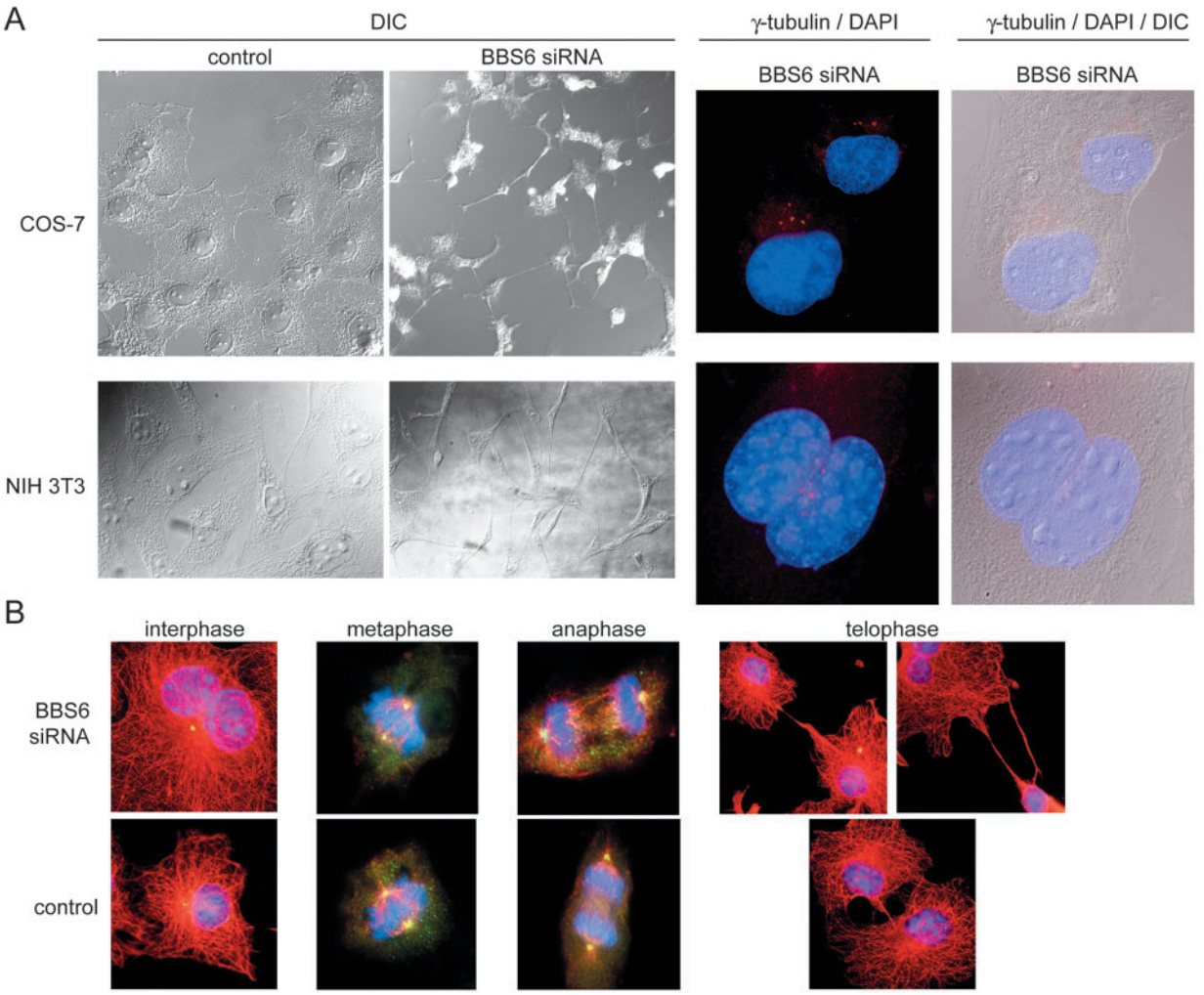

Fig. 7. Silencing of *BBS6* by RNAi in COS-7 and NIH 3T3 cells produces multi-nucleated and multi-centrosomal cells, and cytokinesis defects. (A) DIC images of COS-7 and NIH 3T3 cells 9 days after transfection with *BBS6* siRNA expression vector (pSilencer-BBS6 or pSuper-BBS6, respectively) show interconnected cells with long intercellular bridges as a result of defective cytokinesis. Immunocytochemistry with a γ-tubulin antibody (red) and DAPI staining of nuclei (blue) show that *BBS6* silencing causes bi-nucleated and multi-centrosomal phenotypes in both COS-7 and NIH 3T3 cells. The merged images (right panels) show two nuclei in single cells. (B) Microtubule organization is not significantly altered during cell cycle progression in COS-7 cells transfected with pSilencer-BBS6 (upper panels) compared with cells transfected with pSilencer empty vector (lower panels). Cells were stained with antibodies to α-tubulin (red), γ-tubulin (green) and counterstained with DAPI (blue). Only merged images are shown; yellow indicates overlapping α- and γ-tubulin signals.

(Brummelkamp et al., 2002) targeting a different region of *BBS6*. After selection in G418, we isolated two different clonal lines (A and B) and measured the levels of *BBS6* expression by real-time quantitative RT-PCR. Both lines showed a significant reduction in *BBS6* expression (4- and 16-fold reduction, respectively). In addition, our quantitative immunocytochemistry analysis on both lines A and B revealed that the fluorescent signal of endogenous BBS6 decreased by 2- and 3.5-fold, respectively, and that this decrease is tightly correlated with the cytokinesis and centrosome defects (data not shown). As with the COS-7 cells, we found that *BBS6*-silenced cells displayed a high incidence of cytokinesis-arrested cells with unresolved intercellular bridges (Fig. 7A, bottom panels). This cytokinesis defect in NIH 3T3 cells was reproducible and not observed in control cells transfected with empty pSUPER vector, although it was somewhat less pronounced than that observed in COS-7 cells. This difference, which allowed us to maintain (unhealthy) cell lines, potentially indicates cell-type-specific effects of reducing BBS6 levels. The two *BBS6*-silenced NIH 3T3 cell lines also revealed a significant increase in bi- or multi-nucleated cells compared with control cells (line A: 8.3%, n=361; line B: 10.5%, n=388; control: 2.6%, n=386; Fig. 7A). Finally, siRNA treatment resulted in a greater proportion of cells containing more than two pairs of centrosomes (line A: 13.3%, n=408; line B: 17.5%, n=450; control: 4%, n=719; Fig. 7A).

Altogether, our results indicate that diminishing BBS6 levels in two cell types leads to cytokinesis failure, as well as an accumulation of cells containing abnormal numbers of nuclei and centrosomes. Interestingly, knockdown of *BBS4* similarly leads to a cell division arrest and an accumulation of multi-nucleated and multi-centrosomal cells, probably as a result of

microtubule release (de-anchoring) from the centrosome (Kim et al., 2004). We therefore tested if *BBS6* silencing in COS-7 cells results in alterations in microtubule organization in interphase and dividing cells. Intriguingly, our results show that the microtubule architecture appears normal in *BBS6*-silenced cells (especially compared with *BBS4*-silenced cells), as no conspicuous abnormalities were observed throughout the cell cycle in cells that ultimately fail to undergo cytokinesis (Fig. 7B). Given the presence of BBS6 at the midbody, the observed cytokinesis defects could conceivably be ascribed to a specific role of the chaperonin-like protein in the abscission of the intercellular bridge.

BBS6 is expressed in organs pertinent to BBS and at high levels in ciliated tissues

To shed light on how the centrosomal and cytokinesis defects observed in cultured cells relates to the in vivo function of BBS6 and its link to a pleiotropic disorder that affects numerous tissues, we studied its expression pattern in mouse embryos and tissues. Whole-mount in situ analyses of developing (E10.5-E12) embryos with an RNA probe specific to the *BBS6* transcript revealed prominent staining in the heart, brain, retina and limb buds (Fig. 8A), as well as in the developing neural tube (not shown). This expression pattern reflects the known organs that are affected in BBS patients (i.e. limb buds, polydactyly; heart, congenital heart disease; retina, retinal degeneration; brain and neural tube, neurological phenotypes). In addition, we observed prominent staining in the first and second branchial arches, raising the possibility that mispatterning of these structures might be responsible for the dysmorphic facial and tooth features of BBS patients (Beales et al., 1999). We also used our affinity-purified anti-BBS6 antibody to stain paraffin-embedded tissue sections of mice brain, kidney, retina, olfactory epithelium and the ependymal layer of ventricles (Fig. 8B-F). Interestingly, BBS6 was detected only in restricted regions of these tissue sections, including the ciliated border of renal tubules, the connecting cilium and the inner and outer nuclear layers of retina, and the ciliated layer of olfactory epithelia. These results indicate that BBS6 is preferentially enriched in regions that contain or border ciliated cells, similar to that observed for BBS4 and BBS8 (Ansley et al., 2003; Kim et al., 2004).

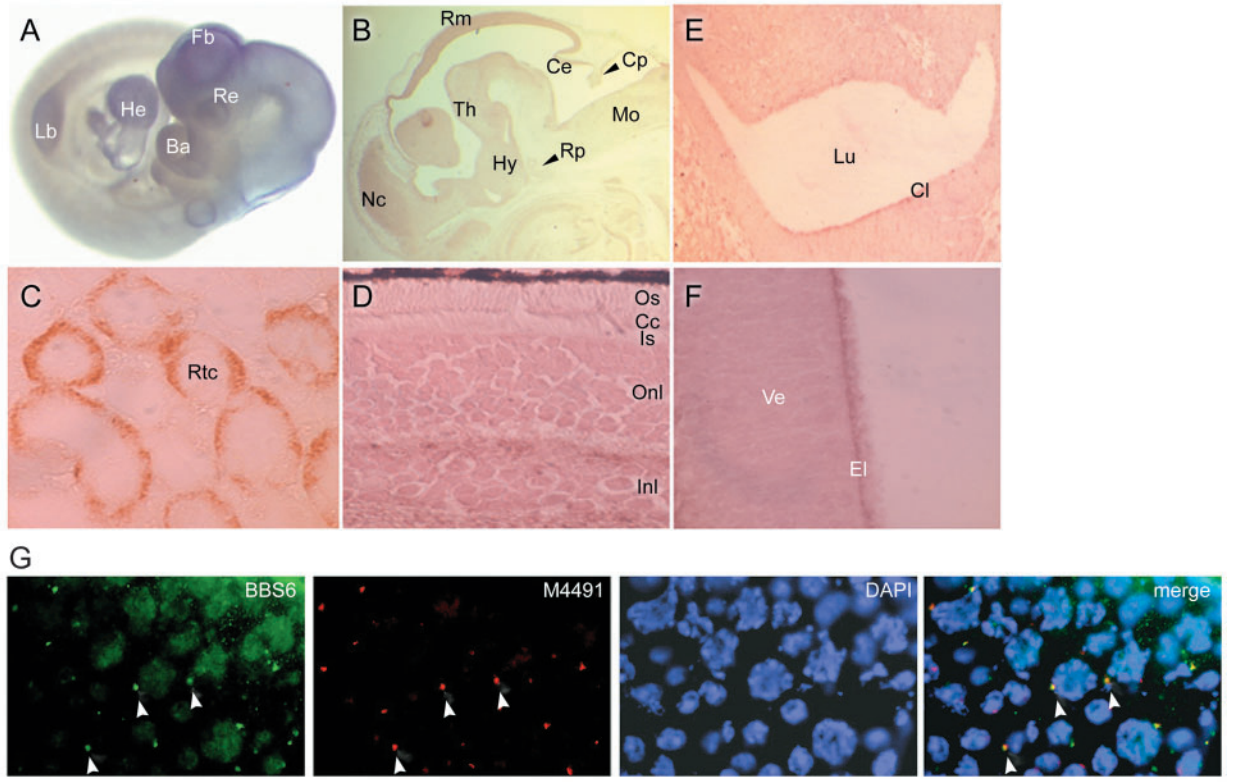

Fig. 8. BBS6 is enriched in organs affected in BBS and in ciliated cells. (A) Wholemount RNA in situ hybridization of an E10 mouse embryo showing strong *BBS6* expression in the forebrain (Fb), retina (Re), branchial arches (Ba), developing heart (He) and limb bud (Lb). (B) Immunohistochemistry using BBS6 antibody; saggital section of a mouse E13.5 brain showing protein staining in the developing nervous system, including the neopallial cortex (Nc), the roof of the midbrain (Rm), the cerebellar primordium (Ce), the choroid plexus (Cp), the hypothalamus (Hy) and Rathke's pouch (Rp). Modest BBS6 protein staining is also detectable in the thalamus (Th) and the medulla oblongata (Mo). (C) In the adult kidney, BBS6 localizes to the ciliated border of renal tubular cells (Rtc). (D) In the adult photoreceptor, BBS6 is detected in the connecting cilium (Cc) and the inner and outer nuclear layers (Inl, Onl) but not the outer or inner segment (Os, Is). (E,F) BBS6 localizes to the ciliated layer of the olfactory epithelium (cl) as well as the ependymal layer (El) of ventricles (Ve); Lu, lumen. (G) A section of mouse testis is stained for BBS6 (green) and the PCM tube (antibody M4491; red). The area shown is taken from the periphery of a semineferous tubule containing both meiotic and spermatogenic cells. BBS6 colocalizes to centrosomes/basal bodies, but not the flagellar axoneme, in spermatogenic cells (see arrowheads). Also shown are nuclei (DAPI stained, blue) and a merged image.

BBS4 has been implicated in the assembly of sperm flagella (Mykytyn et al., 2004). Consistent with this observation, we detected BBS6 in cells undergoing spermatogenesis in mouse testis sections. Fig. 8G shows that BBS6 is confined to the centrosomes/basal bodies in this tissue and is not present along the flagellar axoneme in cells undergoing spermiogenesis. This localization pattern suggests that BBS6 may play an important role in sperm flagellation.

Discussion

We have shown that MKKS/BBS6, a previously uncharacterized chaperonin-like protein linked to the McKusick-Kaufman and Bardet-Biedl syndromes, is a highly divergent member of the CCT chaperonin family that has evolved unique structural and functional properties.

Phylogenetic distribution of BBS6

BBS6 emerged relatively late during the evolution of animals. It is absent from *C. elegans* and *Drosophila* (protostomes), and from unicellular eukaryotes such as *Chlamydomonas reinhardtii* (green alga) and *Saccharomyces cerevisiae* (yeast), but may be broadly distributed in deuterostomes, as it is found in vertebrates as well as the urochordate *C. intestinalis*. This contrasts with other BBS proteins, which appear to exist in all ciliated organisms, from unicellular *Chlamydomonas* and *Tetrahymena*, to the multicellular organisms *C. elegans*, *Drosophila* and humans. This, combined with our findings, suggest that BBS6 co-evolved with, and potentially assists the function or localization of, other protein(s) that emerged in the deuterostome lineage.

BBS6 as a molecular chaperone

Is BBS6 a molecular chaperone? Although the primary structure of BBS6 is clearly similar to that of Group II chaperonins, including the presence of an apical domain protrusion used to encapsulate substrates by CCT and the archaeal chaperonin (see Fig. S1 in supplementary material), several lines of evidence suggest that BBS6 may not function like a bona fide chaperonin that assists protein folding. First, the soluble form of the protein does not form oligomers like other chaperonins, an important distinction considering that oligomerization is widely believed to be a requisite for chaperonin activity (Weber et al., 1998). As the centrosomal localization of BBS6 necessitates only the apical domain (which is unlikely to oligomerize) (Carrascosa et al., 2001), it is possible that BBS6 does not need to form oligomers in the PCM to interact with its binding partner(s)/substrate(s). Furthermore, several residues critical for ATP binding/hydrolysis in other chaperonins are different in BBS6, suggesting that BBS6 may have reduced/absent ATP-dependent conformational changes compared with other chaperonins and thus may not function as other chaperonins (Fig. 1 and Fig. S1 in supplementary material) (see also Ditzel et al., 1998). Despite our efforts, we have not been able to produce soluble or refolded recombinant BBS6 from bacterial or insect expression systems, making it difficult to directly test any potential chaperone or ATP binding/hydrolysis activities.

Effect of patient-associated mutations in BBS6

To investigate the effects of BBS6 mutations found in patients, we expressed in mammalian cells seven different mutant forms of the protein. Four of the BBS6 missense mutants failed to localize to the centrosome, three of which were affected in their apical domain. Combined with our observation that the isolated BBS6 apical domain associates with the centrosome, as does a truncated form of the protein retaining the apical domain, our data suggests that in some BBS patients, the failure of BBS6 to localize to the centrosome may result in disease. This is an important finding, because it provides evidence that the in vivo function of BBS6 is dependent on its association with the centrosome/basal body.

BBS6 in cytokinesis and cilia function

The presence of BBS6 in the PCM of centrosomes and basal bodies suggests that it probably plays a role in association with centrioles. We showed that disruption of this role impacts cytokinesis and produces multi-nucleate, multi-centrosomal cells, but BBS6 may also have more subtle effects on other centrosome/basal body-based functions, including ciliogenesis and cytoskeletal organization. The exact role of BBS6 in cytokinesis and the midbody merits further investigation. Although cleavage furrow formation appears normal in cells treated with *BBS6* siRNAs (Fig. 7B), it is possible that subtle defects have occurred in the organization of microtubules that underlie the intercellular bridge, or in the localization of specific proteins, such as myosin II, which is required for furrow formation and abscission. It is known that membrane trafficking to the furrow is important for assembling the cytokinesis machinery; for example, disruption of clathrin function results in failed cytokinesis (O'Halloran, 2000). Thus, similar to the recruitment of PCM1 by BBS4 to the centrosome, BBS6 at the midbody may recruit proteins required for cytokinesis via microtubule-dependent membrane trafficking. In this respect, it is intriguing that the newly identified BBS3 protein belongs to the ARF/ARL family of small GTP-binding proteins, which are collectively involved in trafficking vesicle-associated proteins (Chiang et al., 2004; Fan et al., 2004).

Given the roles of *C. elegans*, *Chlamydomonas* and murine BBS proteins in the structural integrity of cilia/flagella (Blacque et al., 2004; Kulaga et al., 2004; Li et al., 2004; Mykytyn et al., 2004), we tested the effect of reducing *BBS6* expression by siRNA in ciliated NIH 3T3 cells. We found, however, that compared with empty vector-transfected control cells, *BBS6* silencing did not significantly affect the frequency (*BBS6* knockdown: 10.5%, n=439; control: 10.3%, n=321) nor the gross morphology (average length) of cilia (*BBS6* knockdown: 3.09 μm, n=77; control: 3.18 μm, n=138). This observation raises several possibilities: (1) siRNA treatment of the cells is ineffective in producing a ciliary phenotype, or (2) the cilia are affected in function but not structure, or (3) a putative ciliary dysfunction in BBS6 patients results from an indirect effect of the cytokinesis defect on the function of ciliated epithelial cells/tissues. These possible scenarios will probably need to be investigated using a *BBS6* knockout mouse model system.

In conclusion, our study shows that BBS6, a chaperonin-like protein related to CCT, plays specialized role(s) at the

pericentriolar material of the centrosome, and suggests that centrosomal/basal body and cytokinesis defects in ciliated tissues may be responsible for the pathogenicity of Bardet-Biedl syndrome.

This research has been funded by the Canadian Institutes of Health Research (CIHR) and the Heart and Stroke Foundation of B.C. and Yukon (HSFBC&Y) (M.R.L.), the Natural Sciences and Engineering Research Council of Canada (NSERC) (J.B.R.), and the National Institute of Child Health and Development, National Institutes of Health grant HD042260 (N.K.). M.R.L. is the recipient of Michael Smith Foundation for Health Research (MSFHR) and CIHR scholar awards. P.L.B. is a Wellcome Trust Senior Research Fellow. Y.Y.O. is a CIHR postdoctoral fellow, J.C.K. is supported by MSFHR, and M.A.E. by HSF Canada and CIHR.

References

Ansley, S. J., Badano, J. L., Blacque, O. E., Hill, J., Hoskins, B. E., Leitch, C. C., Kim, J. C., Ross, A. J., Eichers, E. R., Teslovich, T. M. et al. (2003). Basal body dysfunction is a likely cause of pleiotropic Bardet-Biedl syndrome. *Nature* **425**, 628-633.

Archibald, J. M., Logsdon, J. M. and Doolittle, W. F. (1999). Recurrent paralogy in the evolution of archaeal chaperonins. *Curr. Biol.* **9**, 1053-1056.

Archibald, J. M., Logsdon, J. M., Jr and Doolittle, W. F. (2000). Origin and evolution of eukaryotic chaperonins: phylogenetic evidence for ancient duplications in CCT genes. *Mol. Biol. Evol.* **17**, 1456-1466.

Badano, J. L., Ansley, S. J., Leitch, C. C., Lewis, R. A., Lupski, J. R. and Katsanis, N. (2003). Identification of a novel Bardet-Biedl syndrome protein, BBS7, that shares structural features with BBS1 and BBS2. *Am. J. Hum. Genet.* **72**, 650-658.

Beales, P. L., Elcioglu, N., Woolf, A. S., Parker, D. and Flinter, F. A. (1999). New criteria for improved diagnosis of Bardet-Biedl syndrome: results of a population survey. *J. Med. Genet.* **36**, 437-446.

Blacque, O. E., Reardon, M. J., Li, C., McCarthy, J., Mahjoub, M. R., Ansley, S. J., Badano, J. L., Mah, A. K., Beales, P. L., Davidson, W. S. et al. (2004). Loss of *C. elegans* BBS-7 and BBS-8 protein function results in cilia defects and compromised intraflagellar transport. *Genes Dev.* **18**, 1630-1642.

Brummelkamp, T. R., Bernards, R. and Agami, R. (2002). A system for stable expression of short interfering RNAs in mammalian cells. *Science* **296**, 550-553.

Carrascosa, J. L., Llorca, O. and Valpuesta, J. M. (2001). Structural comparison of prokaryotic and eukaryotic chaperonins. *Micron* **32**, 43-50.

Chiang, A. P., Nishimura, D., Searby, C., Elbedour, K., Carmi, R., Ferguson, A. L., Secrist, J., Braun, T., Casavant, T., Stone, E. M. et al. (2004). Comparative genomic analysis identifies an ADP-ribosylation factor-like gene as the cause of Bardet-Biedl syndrome (BBS3). *Am. J. Hum. Genet.* **75**, 475-484.

Dammermann, A. and Merdes, A. (2002). Assembly of centrosomal proteins and microtubule organization depends on PCM-1. *J. Cell Biol.* **159**, 255-266.

Ditzel, L., Lowe, J., Stock, D., Stetter, K. O., Huber, H., Huber, R. and Steinbacher, S. (1998). Crystal structure of the thermosome, the archaeal chaperonin and homolog of CCT. *Cell* **93**, 125-138.

Fan, Y., Esmail, M. A., Ansley, S. J., Blacque, O. E., Boroevich, K., Ross, A. J., Moore, S. J., Badano, J. L., May-Simera, H., Compton, D. S. et al. (2004). Mutations in a member of the Ras superfamily of small GTP-binding proteins causes Bardet-Biedl syndrome. *Nat. Genet.* **36**, 989-993.

Gascuel, O. (1997). BIONJ: an improved version of the NJ algorithm based on a simple model of sequence data. *Mol. Biol. Evol.* **14**, 685-695.

Gutsche, I., Essen, L. O. and Baumeister, W. (1999). Group II chaperonins: new TRiC(k)s and turns of a protein folding machine. *J. Mol. Biol.* **293**, 295-312.

Hartl, F. U. and Hayer-Hartl, M. (2002). Molecular chaperones in the cytosol: from nascent chain to folded protein. *Science* **295**, 1852-1858.

Horwich, A. L. and Willison, K. R. (1993). Protein folding in the cell: functions of two families of molecular chaperone, hsp 60 and TF55-TCP1. *Philos. Trans R Soc. Lond. B Biol. Sci.* **339**, 313-325; discussion 325-316.

Hynes, G., Kubota, H. and Willison, K. R. (1995). Antibody characterisation of two distinct conformations of the chaperonin-containing TCP-1 from mouse testis. *FEBS Lett.* **358**, 129-132.

Katsanis, N. (2004). The oligogenic properties of Bardet-Biedl syndrome. *Hum. Mol. Genet.* 13, Spec. No. 1, R65-71.

Katsanis, N., Beales, P. L., Woods, M. O., Lewis, R. A., Green, J. S., Parfrey, P. S., Ansley, S. J., Davidson, W. S. and Lupski, J. R. (2000). Mutations in MKKS cause obesity, retinal dystrophy and renal malformations associated with Bardet-Biedl syndrome. *Nat. Genet.* **26**, 67-70.

Kim, J. C., Badano, J. L., Sibold, S., Esmail, M. A., Hill, J., Hoskins, B. E., Leitch, C. C., Venner, K., Ansley, S. J., Ross, A. J. et al. (2004). The Bardet-Biedl protein BBS4 targets cargo to the pericentriolar region and is required for microtubule anchoring and cell cycle progression. *Nat. Genet.* **36**, 462-470.

Kubota, H., Hynes, G. and Willison, K. (1995). The chaperonin containing *t*-complex polypeptide 1 (TCP-1). Multisubunit machinery assisting in protein folding and assembly in the eukaryotic cytosol. *Eur. J. Biochem.* **230**, 3-16.

Kulaga, H. M., Leitch, C. C., Eichers, E. R., Badano, J. L., Lesemann, A., Hoskins, B. E., Lupski, J. R., Beales, P. L., Reed, R. R. and Katsanis, N. (2004). Loss of BBS proteins causes anosmia in humans and defects in olfactory cilia structure and function in the mouse. *Nat. Genet.* **36**, 994-998.

Leroux, M. R. and Hartl, F. U. (2000). Protein folding: versatility of the cytosolic chaperonin TRiC/CCT. *Curr. Biol.* **10**, R260-264.

Li, J. B., Gerdes, J. M., Haycraft, C. J., Fan, Y., Teslovich, T. M., May-Simera, H., Li, H., Blacque, O. E., Li, L., Leitch, C. C. et al. (2004). Comparative genomics identifies a flagellar and basal body proteome that includes the *BBS5* human disease gene. *Cell* **117**, 541-552.

Mack, G. J., Rees, J., Sandblom, O., Balczon, R., Fritzler, M. J. and Rattner, J. B. (1998). Autoantibodies to a group of centrosomal proteins in human autoimmune sera reactive with the centrosome. *Arthritis Rheum.* **41**, 551-558.

Meyer, A. S., Gillespie, J. R., Walther, D., Millet, I. S., Doniach, S. and Frydman, J. (2003). Closing the folding chamber of the eukaryotic chaperonin requires the transition state of ATP hydrolysis. *Cell* **113**, 369-381.

Mykytyn, K., Braun, T., Carmi, R., Haider, N. B., Searby, C. C., Shastri, M., Beck, G., Wright, A. F., Iannaccone, A., Elbedour, K. et al. (2001). Identification of the gene that, when mutated, causes the human obesity syndrome BBS4. *Nat. Genet.* **28**, 188-191.

Mykytyn, K., Nishimura, D. Y., Searby, C. C., Shastri, M., Yen, H. J., Beck, J. S., Braun, T., Streb, L. M., Cornier, A. S., Cox, G. F. et al. (2002). Identification of the gene (BBS1) most commonly involved in Bardet-Biedl syndrome, a complex human obesity syndrome. *Nat. Genet.* **31**, 435-438.

Mykytyn, K., Mullins, R. F., Andrews, M., Chiang, A. P., Swiderski, R. E., Yang, B., Braun, T., Casavant, T., Stone, E. M. and Sheffield, V. C. (2004). Bardet-Biedl syndrome type 4 (*BBS4*)-null mice implicate Bbs4 in flagella formation but not global cilia assembly. *Proc. Natl. Acad. Sci. USA* **101**, 8664-8669.

Nishimura, D. Y., Searby, C. C., Carmi, R., Elbedour, K., van Maldergem, L., Fulton, A. B., Lam, B. L., Powell, B. R., Swiderski, R. E., Bugge, K. E. et al. (2001). Positional cloning of a novel gene on chromosome 16q causing Bardet-Biedl syndrome (BBS2). *Hum. Mol. Genet.* **10**, 865-874.

O'Halloran, T. J. (2000). Membrane traffic and cytokinesis. *Traffic* **1**, 921-926.

Ou, Y. Y. and Rattner, J. B. (2000). A subset of centrosomal proteins are arranged in a tubular conformation that is reproduced during centrosome duplication. *Cell Motil. Cytoskeleton* **47**, 13-24.

Ou, Y. Y., Zhang, M., Chi, S., Matyas, J. R. and Rattner, J. B. (2003). Higher order structure of the PCM adjacent to the centriole. *Cell Motil. Cytoskeleton* **55**, 125-133.

Pappenberger, G., Wilsher, J. A., Roe, S. M., Counsell, D. J., Willison, K. R. and Pearl, L. H. (2002). Crystal structure of the CCTγ apical domain: implications for substrate binding to the eukaryotic cytosolic chaperonin. *J. Mol. Biol.* **318**, 1367-1379.

Piel, M., Nordberg, J., Euteneuer, U. and Bornens, M. (2001). Centrosome-dependent exit of cytokinesis in animal cells. *Science* **291**, 1550-1553.

Siegers, K., Waldmann, T., Leroux, M. R., Grein, K., Shevchenko, A., Schiebel, E. and Hartl, F. U. (1999). Compartmentation of protein folding *in vivo*: sequestration of non-native polypeptide by the chaperonin-GimC system. *EMBO J.* **18**, 75-84.

Siegert, R., Leroux, M. R., Scheufler, C., Hartl, F. U. and Moarefi, I. (2000). Structure of the molecular chaperone prefoldin: unique interaction of multiple coiled coil tentacles with unfolded proteins. *Cell* **103**, 621-632.

Slavotinek, A. M., Stone, E. M., Mykytyn, K., Heckenlively, J. R., Green,

J. S., Heon, E., Musarella, M. A., Parfrey, P. S., Sheffield, V. C. and Biesecker, L. G. (2000). Mutations in MKKS cause bardet-biedl syndrome. *Nat. Genet.* **26**, 15-16.

Stone, D. L., Slavotinek, A., Bouffard, G. G., Banerjee-Basu, S., Baxevanis, A. D., Barr, M. and Biesecker, L. G. (2000). Mutation of a gene encoding a putative chaperonin causes McKusick-Kaufman syndrome. *Nat. Genet.* **25**, 79-82.

Strimmer, K. and von Haeseler, A. (1996). Quartet puzzling: a quartet maximum-likelihood method for reconstructing tree topologies. *Mol. Biol. Evol.* **13**, 964-969.

Tsvetkov, L., Xu, X., Li, J. and Stern, D. F. (2003). Polo-like kinase 1 and Chk2 interact and co-localize to centrosomes and the midbody. *J. Biol. Chem.* **278**, 8468-8475.

Vainberg, I. E., Lewis, S. A., Rommelaere, H., Ampe, C., Vandekerckhove, J., Klein, H. L. and Cowan, N. J. (1998). Prefoldin, a chaperone that delivers unfolded proteins to cytosolic chaperonin. *Cell* **93**, 863-873.

Valpuesta, J. M., Martin-Benito, J., Gomez-Puertas, P., Carrascosa, J. L. and Willison, K. R. (2002). Structure and function of a protein folding machine: the eukaryotic cytosolic chaperonin CCT. *FEBS Lett.* **529**, 11-16.

Vaughan, K. T. and Vallee, R. B. (1995). Cytoplasmic dynein binds dynactin through a direct interaction between the intermediate chains and p150Glued. *J. Cell Biol.* **131**, 1507-1516.

Weber, F., Keppel, F., Georgopoulos, C., Hayer-Hartl, M. K. and Hartl, F. U. (1998). The oligomeric structure of GroEL/GroES is required for biologically significant chaperonin function in protein folding. *Nat. Struct. Biol.* **5**, 977-985.